Chemistry–A European Journal
Research Article
doi.org/10.1002/chem.202203181
Chemistry Europe
European Chemical Societies Publishing
www.chemeurj.org

Check for updates

Terminal Au–N and Au–O Units in Organometallic Frames

Alberto Pérez-Bitrián,[a] Santiago Alvarez,*[b] Miguel Baya,[a] Jorge Echeverría,[a] Antonio Martín,[a] Jesús Orduna,[c] and Babil Menjón*[a]

Dedicated to Prof. Dr. Juan Forniés on the occasion of his 75th birthday.

Abstract: Since gold is located well beyond the oxo wall, chemical species with terminal Au–N and Au–O units are extremely rare and limited to low coordination numbers. We report here that these unusual units can be trapped within a suitable organometallic frame. Thus, the terminal auronitrene and auroxyl derivatives $[(CF_3)_3AuN]^-$ and $[(CF_3)_3AuO]^-$ were identified as local minima by calculation. These open-shell, high-energy ions were experimentally detected by tandem mass spectrometry (MS^2): They respectively arise by N_2 or NO_2 dissociation from the corresponding precursor species $[(CF_3)_3Au(N_3)]^-$ and $[(CF_3)_3Au(ONO_2)]^-$ in the gas phase. Together with the known fluoride derivative $[(CF_3)_3AuF]^-$, they form an interesting series of isoleptic and alloelectronic complexes of the highly acidic organogold(III) moiety $(CF_3)_3Au$ with singly charged anions X^- of the most electronegative elements (X = F, O, N). Ligand-field inversion in all these $[(CF_3)_3AuX]^-$ species results in the localization of unpaired electrons at the N and O atoms.

Introduction

Terminal nitride and oxo ligands are particularly favored in electron-poor early transition metals (TMs).[1,2] Their stability, however, decreases markedly in electron-rich late TMs as to justify the "oxo wall" concept.[3] This concept is extensible to nitrides, but has no meaning for fluorides.[4] The oxo wall position depends on the molecular symmetry: It is established between Groups 8 and 9 for six-coordinate metal oxo complexes with tetragonal symmetry (i.e., compressed octahedral), but is shifted rightwards for lower coordination numbers.[3a] Thus, the tetrahedral Mes_3IrO[5] and the square-planar (PNP)IrO[6] complexes are well established. A diamagnetic Pt(IV) complex with a (strongly bent) terminal Pt=O unit,[7] aroused some controversy though.[8] Very high oxidation states are also known to favor M–O multiple bonds at the right edge of the TM series, as in the $(IrO_4)^+$ cation, which is the only Ir(IX) entity experimentally detected to date.[9] The species $(PtO_4)^{2+}$, $(PtNO_3)^+$, PtN_2O_2 and $(PtN_3O)^-$ have also been identified as metastable energy minima by calculation.[10]

Gold is the least oxophilic metal.[11] Accordingly, compounds containing terminal AuO units are only found at the unimolecular level, i.e., either in the gas phase or in inert solid matrices (Scheme 1).[12] They all exhibit low coordination numbers (<4): $(AuO)^{q+}$ ($q = -1, 0, 1, 2$),[1,13] $OAuF_n$ ($n = 1, 2$),[14] $(OAuO)^{q-}$ ($q = 0, 1$),[1,13] and $[OAu(OBO)]^-$,[15] while the constitution of the $(AuO_4)^+$ cation is currently unknown.[16] The recent synthesis of a terminal Pt–N unit in the fascinating (PNP)PtN complex[17] prompted us to move a step further to Group 11 and explore the possibility of existence of related Au–N and Au–O units.

In previous work, we have identified the $(CF_3)_3Au$ moiety as a strong Lewis acid[18] with distinct stereochemical stability and a marked reluctance to undergo reductive elimination.[19] Considering all these advantageous features, we conjectured that this well-behaved perfluorinated organogold moiety might provide a suitable frame for terminal AuN and AuO units well beyond the oxo wall.

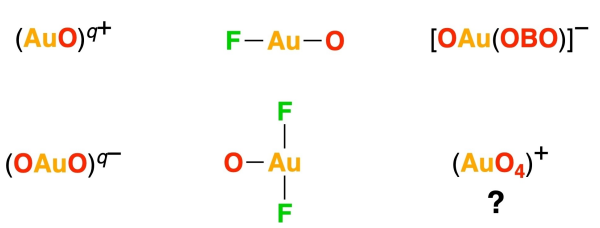

Scheme 1. Structural formulas of the experimentally detected species with terminal AuO units.

[a] Dr. A. Pérez-Bitrián, Dr. M. Baya, Dr. J. Echeverría, Dr. A. Martín, Dr. B. Menjón
Instituto de Síntesis Química y Catálisis Homogénea (iSQCH)
CSIC-Universidad de Zaragoza
50009 Zaragoza (Spain)
E-mail: menjon@ctq.csic.es

[b] Prof. Dr. S. Alvarez
Departament de Química Inorgànica i Orgànica
Facultat de Química, Universitat de Barcelona
08028 Barcelona (Spain)
E-mail: santiago.alvarez@qi.ub.es

[c] Dr. J. Orduna
Instituto de Nanociencia y Materiales de Aragón (INMA)
CSIC-Universidad de Zaragoza
50009 Zaragoza (Spain)

Supporting information for this article is available on the WWW under https://doi.org/10.1002/chem.202203181

© 2022 The Authors. Chemistry - A European Journal published by Wiley-VCH GmbH. This is an open access article under the terms of the Creative Commons Attribution Non-Commercial NoDerivs License, which permits use and distribution in any medium, provided the original work is properly cited, the use is non-commercial and no modifications or adaptations are made.

© 2022 The Authors. Chemistry - A European Journal published by Wiley-VCH GmbH

15213765, 2023, 8, Downloaded from https://chemistry-europe.onlinelibrary.wiley.com/doi/10.1002/chem.202203181 by Universidad De Zaragoza, Wiley Online Library on [28/02/2023]. See the Terms and Conditions (https://onlinelibrary.wiley.com/terms-and-conditions) on Wiley Online Library for rules of use; OA articles are governed by the applicable Creative Commons License

Results and Discussion

The nitrogen system

We first prepared the gold(III) azide complex $[PPh_4][(CF_3)_3Au(N_3)]$ (**1**) from the iodo-derivative $[PPh_4][(CF_3)_3AuI]$[19] by ligand exchange. Compound **1** was characterized by analytical, spectroscopic and structural methods (see Experimental). Furthermore, the crystal and molecular structures of the $[Ph_3PCH_2Ph][(CF_3)_3Au(N_3)]$ (**1′**) salt were established by single-crystal X-ray diffraction (sc-XRD) methods.[20] The structure of the $[(CF_3)_3Au(N_3)]^-$ anion in **1′** (Scheme 2; Table S2) is similar to that previously established for the homologous silver complex $[(CF_3)_3Ag(N_3)]^-$.[21] The Au-N^α bond length in **1′** (204.4(5) pm) is also indistinguishable from the Pt-N^α distance found in the related Pt compound (PNP)Pt(N_3): 203.1(5).[17] However, the higher ν_a(NNN) frequency observed in the IR spectrum of the gold compound **1** (2061 cm^{-1}) when compared to that of the silver counterpart (2042 cm^{-1}) might suggest higher covalent character in the Au–N_3 bond.[22] This difference will have important consequences in the present study, as we will see below. The gold compound is substantially more stable (265 °C, dec.) than the silver homologue (92 °C, dec.).[21]

Having isolated compound **1** in pure form, we studied the unimolecular decomposition paths of the $[(CF_3)_3Au(N_3)]^-$ anion in the gas phase by multistage mass spectrometry (MS^n) under collision-induced dissociation (CID) conditions (Figures S6–S9). The main path involves dissociation of the N_3 ligand and one of the CF_3 groups affording the homoleptic organogold(I) anion $[CF_3AuCF_3]^-$ (Scheme 2). No ionic dissociation of $(N_3)^-$ involving heterolytic Au-N_3 cleavage was experimentally detected.[23,24] The sought N_2 dissociation takes place to only a limited extent furnishing $[(CF_3)_3AuN]^-$ as a minor product. Finally, double dissociation of CF_3 renders the lineal azide gold(I) complex $[CF_3AuN_3]^-$. This compound was also prepared in solution and its structure was established (sc-XRD) in the salt $[PPh_4][CF_3AuN_3]$ (**2**: Scheme 2; Table S4).[20] It releases N_2 in the gas phase giving rise to the $[CF_3AuN]^-$ anion as the main product (Scheme 2). Species $[(CF_3)_3AuN]^-$ and $[CF_3AuN]^-$ are extremely rare cases of terminal Au–N units. It is worth noting that no homologous silver complex $[(CF_3)_3AgN]^-$ was observed in the fragmentation of the corresponding parent species $[(CF_3)_3Ag(N_3)]^-$ in the gas phase under similar CID conditions. The different behavior observed for Ag and Au nicely correlates with the higher covalent character of the Au–N_3 bond in the corresponding parent complex as already pointed out by the variation in their respective ν_a(NNN) frequency values (see above).

The oxygen system

In order to extend our results to oxygen, a suitable precursor was needed. The nitrate complex $[PPh_4][(CF_3)_3Au(ONO_2)]$ (**3**) was prepared in a similar way as the azide complex **1** (see Experimental) and was isolated as a white solid in good yield (79%). Compound **3** was characterized by analytical and spectroscopic methods. The molecular structure of the anion was also established by sc-XRD on single crystals of the salt

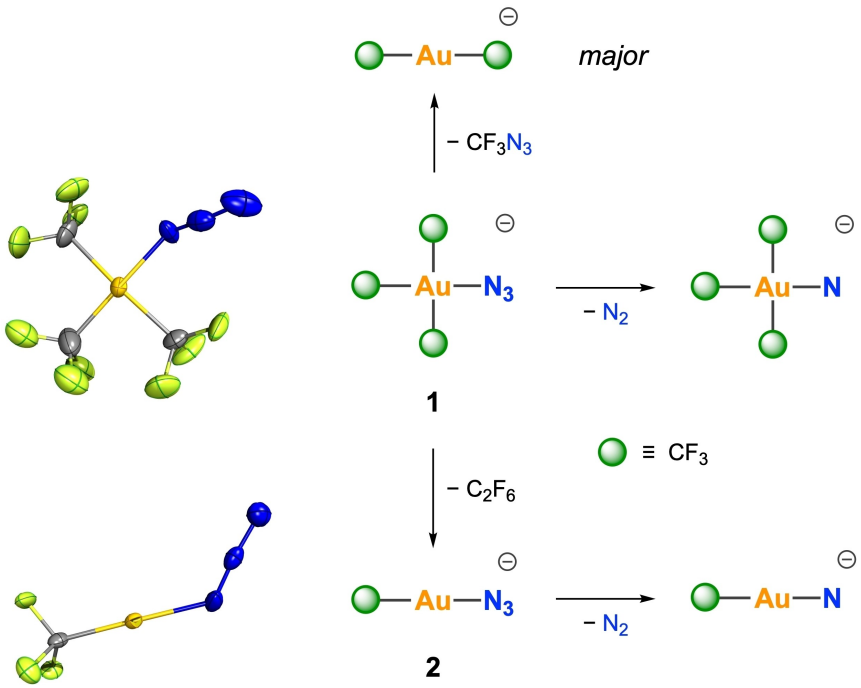

Scheme 2. Fragmentation channels of the $[(CF_3)_3Au(N_3)]^-$ anion in the gas phase under CID conditions. Multistage mass spectra (MS^n) are given in Figures S6–S9. Energies calculated for the different dissociation paths are given in Scheme S1. Shown here are also displacement-ellipsoid diagrams (50% probability) of the $[(CF_3)_3Au(N_3)]^-$ and $[CF_3AuN_3]^-$ anions as found in single crystals of **1′** and **2**, respectively.[20] Both anions undergo CF_2 extrusion as an additional fragmentation channel in the gas phase (not shown here for clarity). No ionic dissociation of N_3^- was experimentally observed (Q-TOF).[23]

© 2022 The Authors. Chemistry - A European Journal published by Wiley-VCH GmbH

15213765, 2023, 8, Downloaded from https://chemistry-europe.onlinelibrary.wiley.com/doi/10.1002/chem.202203181 by Universidad De Zaragoza, Wiley Online Library on [28/02/2023]. See the Terms and Conditions (https://onlinelibrary.wiley.com/terms-and-conditions) on Wiley Online Library for rules of use; OA articles are governed by the applicable Creative Commons License

15213765, 2023, 8, Downloaded from https://chemistry-europe.onlinelibrary.wiley.com/doi/10.1002/chem.202203181 by Universidad De Zaragoza, Wiley Online Library on [28/02/2023]. See the Terms and Conditions (https://onlinelibrary.wiley.com/terms-and-conditions) on Wiley Online Library for rules of use; OA articles are governed by the applicable Creative Commons License

$[Ph_3PCH_2Ph][(CF_3)_3Au(ONO_2)]$ (**3′**).[20] In the square-planar anion, the nitrato group acts as a terminal, monodentate ligand (Scheme 3; Table S6) with a Au–ONO_2 bond distance [209.0(4) pm av.] comparable to that found in (C&N)Au-$(CH_2Ac)(ONO_2)$: 212.8(3) pm.[25] The metrical similarity can be attributed to the nitrato-κ*O* ligand being located in both cases *trans* to an organyl group (CF_3 or aryl) with considerable *trans* influence.[26] Accordingly, the observed Au–O bond distance in **3′** is much longer than observed in the homoleptic nitrate complexes $(NO)[Au(NO_3)_4]$ [200.2(7) pm av.],[27] $(NO_2)[Au(NO_3)_4]$ (199.8 pm av.),[28] and $K[Au(NO_3)_4]$ [200(2) pm av.].[29] The N–OAu bond distance in **3′** [130.9(7) pm av.] is substantially longer than the terminal N–O bonds [123.0(7) pm av.], the latter being just marginally longer than the N–O bond distance in gaseous NO_2: 119.5(3) pm.[30] This difference evidences that the N–OAu bond is significantly weaker than the terminal N–O bond and therefore prone to undergo cleavage under NO_2 dissociation. This point was confirmed by experiment.

The unimolecular dissociation of the $[(CF_3)_3Au(ONO_2)]^-$ anion in the gas phase under CID conditions (Scheme 3) bears much similarity with the azide complex **1** just discussed (Scheme 2). In complex **3**, however, dissociation of the $(NO_3)^-$ ion was observed to occur in Q-TOF experiments.[23] This path involving the heterolytic cleavage of the Au–O bond may be considered as the standard channel for monodentate nitrate complexes, in line with the well-established role of the nitrate ion as a good leaving group in TM chemistry.[31] Dissociation paths leading to linear organogold(I) anions are here minor channels. The main dissociation path involves NO_2 release with formation of $[(CF_3)_3AuO]^-$ (Scheme 3). The preferential formation of this anion indicates substantial stability and involves a less common breaking of a metal nitrate.

Nitrate is a highly electronegative group (estimated χ 3.91)[32] able to form countless ionic salts with a plethora of electropositive cations and also to bind covalently to electronegative elements.[33] Simple nitrates $XONO_2$ with a polar X–O bond, but with predominantly covalent character have been the object of thorough investigation in main-group elements (X = H, CH_3, CF_3, $SiMe_3$, etc.).[33] Among them all, the so-called halogen nitrates[34] are of particular importance since $XONO_2$ molecules (X = halogen) act as reservoirs of atmospheric XO and NO_2 radical species.[35] Different contributions of ionic, $X^+/(NO_3)^-$, and radical, $XO^\bullet/^\bullet NO_2$, bonding models are involved in each case depending on the electronegativity of X.[33] In these molecules, the XO–NO_2 single bond is by far the weakest bond, as observed also in the organogold(III) complex **3′** (see above). Our experimental detection of $[(CF_3)_3AuO]^-$ following the radical dissociation pattern is in line with all these precedents, especially considering that gold is the most electronegative metal (χ 2.4).[36] The observed radical splitting of the AuO–NO_2 unit in **3** discloses important covalent contribution to the Au–O bond, and provides additional evidence for gold behaving as a pseudohalogen.[36]

Dissociation of NO_2 from the nitrate complex **3** involves reduction to N(IV) and requires concomitant oxidation of the organogold moiety. The conventional rules to calculate oxidation states assume that, except when bound to F, a terminal oxygen atom should be invariably taken as an oxo anion O^{2-}.[37] The blind application of this convention based on a single electronegativity value for each chemical element would result in an Au(IV) species. Given the notorious lack of well-established Au(IV) compounds, a thorough analysis of the electronic structure of this unusual species seemed appropriate. We extended our calculation to the aforementioned $[(CF_3)_3AuN]^-$ derivative, as well as to the known fluoride complex

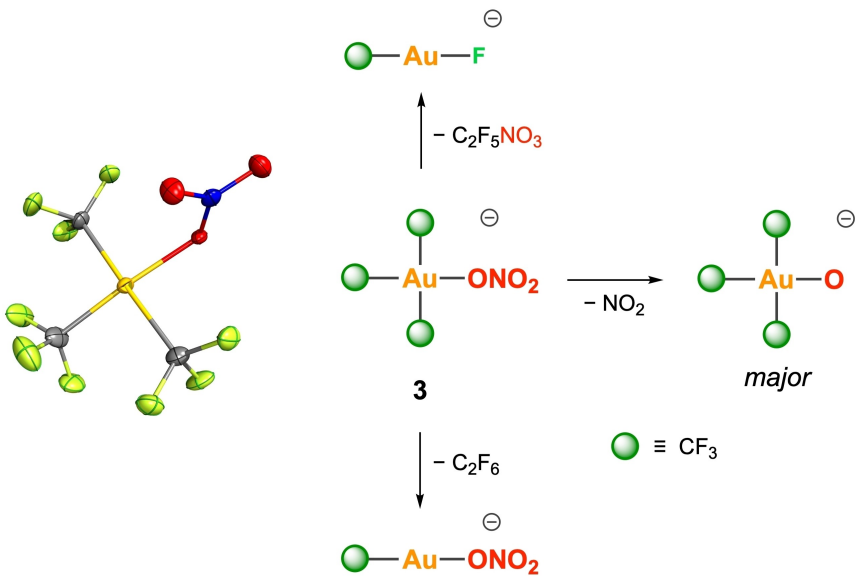

Scheme 3. Fragmentation channels of the $[(CF_3)_3Au(ONO_2)]^-$ anion in the gas phase under CID conditions. Multistage mass spectra (MS^n) are given in Figures S11 and S12. Energies calculated for the different dissociation paths are given in Scheme S2. Shown here is also the displacement-ellipsoid diagram (50% probability) of the $[(CF_3)_3Au(ONO_2)]^-$ anion as found in single crystals of **3′**.[20] Ionic dissociation of NO_3^- is additionally observed (Q-TOF).[23]

© 2022 The Authors. Chemistry - A European Journal published by Wiley-VCH GmbH

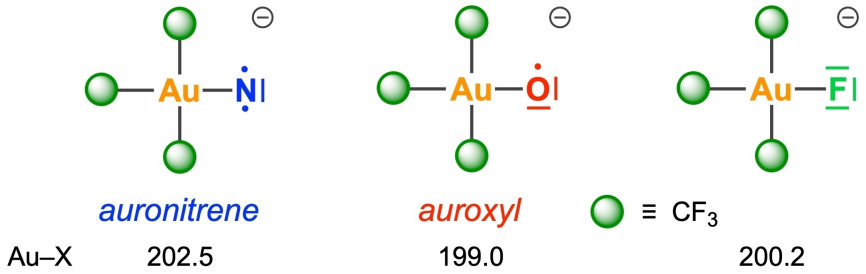

Scheme 4. Lewis structures of the isoleptic and alloelectronic $[(CF_3)_3AuX]^-$ series (X = N, O, F) with calculated Au–X distances [pm] indicated. The electronic structure of the open-shell complexes is described in detail in the Supporting Information (Figures S16 and S17).

$[(CF_3)_3AuF]^-$.[19] They all form an interesting series of isoleptic and alloelectronic species: $[(CF_3)_3AuX]^-$ (X = N, O, F). Following our calculations, they are invariably square planar with similar Au–X bond distances suggesting single bonds (Scheme 4).

Electronic structure of the terminal AuN and AuO units

The electronic structure of the open-shell anions $[(CF_3)_3AuN]^-$ and $[(CF_3)_3AuO]^-$ was ascertained with the help of CAS(n,6) calculations (n = 8, 9 for X=N and O, respectively) including ZORA relativistic corrections for the Au atom (see Supporting Information for details). CASSCF calculations have disclosed that the electronic ground state of the $[(CF_3)_3AuN]^-$ complex is virtually monoconfigurational, with the two unpaired electrons located in the b_2 and $2b_1$ MOs, which are composed mainly of the N(p_x) and N(p_y) atomic orbitals, respectively (Figure S16 and Table S7). On the other hand, for the $[(CF_3)_3AuO]^-$ complex only two configurations account for 94% of the CAS wavefunction, namely those in which the unpaired electron is located in the MOs $1b_1$ and $2b_1$, respectively (Figure S17 and Table S8).

A triplet state was identified as the lowest minimum for the $[(CF_3)_3AuN]^-$ anion (S = 1) with most spin density located on the N atom (Figure 1a) with a cylindrical distribution resulting from the half-occupation of the two N(p) π orbitals. This pattern suggests that the compound should be regarded as an auronitrene. In a similar way, the SOMO of the open-shell species $[(CF_3)_3AuO]^-$ ($S = {}^1/_2$) exhibits Au–O π* character with most spin density located on the O atom (Figure 1b). We conclude therefore that the $[(CF_3)_3AuO]^-$ anion should be viewed as an oxyl ($O^{\bullet -}$) complex of the organogold(III) moiety

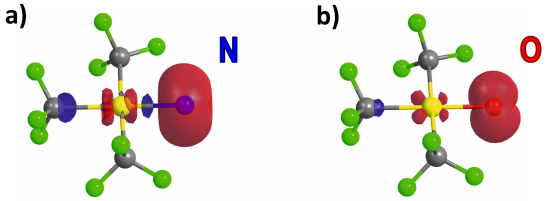

Figure 1. Spin density contour of the square-planar anions a) $[(CF_3)_3AuN]^-$ and b) $[(CF_3)_3AuO]^-$ calculated at the DFT/M06/def2-TZVPD level of theory (isovalue: 0.005).

$(CF_3)_3Au$ rather than an oxo-derivative of Au(IV).[38] Apparently, the oxyl ligand is unable to get its missing electron from the Au(III) center. This means that an Au(IV) center should, in turn, be able to oxidize an oxo ligand by shifting the electronic hole to the O 2p orbitals.[39] Finally, the fluoro complex $[(CF_3)_3AuF]^-$ has the expected closed-shell electronic structure (S = 0). In all three $[(CF_3)_3AuX]^-$ compounds, the metal d orbitals contribute little to the frontier MOs, which are rather involved in the Au–X bonding MOs (Figures S16 and S17). This arrangement is typical of inverted ligand field,[40] as it has been found in related compounds of coinage metals.[21,41] as well as in other highly-covalent late-TM systems. Given the Au–X □* character of the SOMOs, the formal bond order of the Au–N and Au–O bonds is 2 and 1.5, respectively. Taking into consideration all the aforementioned structural and electronic properties, we conclude that the $[(CF_3)_3AuX]^-$ ions are to be considered as complexes of the $(CF_3)_3Au$ moiety with a singly-charged X^- anion (X = N, O, F).

Conclusion

Collision-induced dissociation (CID) of the azide complex $[(CF_3)_3Au(N_3)]^-$ in the gas phase proceeds with N_2 loss and formation of the auronitrene $[(CF_3)_3AuN]^-$ (Scheme 2). In a similar way, the nitrato complex $[(CF_3)_3Au(ONO_2)]^-$ gives rise to the auroxyl complex $[(CF_3)_3AuO]^-$ under NO_2 dissociation (Scheme 3). Single Au–N and Au–O bonds are calculated for the corresponding terminal units with triplet and doublet spin states, respectively, and most spin density located on the non-metal atom (Figure 1). Consequently, these extremely rare cases of terminal Au–N and Au–O bonds boldly defy the conventional rules to assign oxidation states. Our results reinforce the picture of gold as a pseudohalogen. Further studies aiming to detect these high-energy species in the condensed phase are ongoing.

Experimental Section

General procedures and materials: Unless otherwise indicated, the reactions and manipulations were carried out under purified argon using Schlenk techniques. Previously degassed solvents were dried using an MBraun SPS-800 System (CH_2Cl_2, Et_2O, *n*-hexane) or over activated 3 Å molecular sieves (Me_2CO, MeCN). The square-planar

© 2022 The Authors. Chemistry - A European Journal published by Wiley-VCH GmbH

15213765, 2023, 8, Downloaded from https://chemistry-europe.onlinelibrary.wiley.com/doi/10.1002/chem.202203181 by Universidad De Zaragoza, Wiley Online Library on [28/02/2023]. See the Terms and Conditions (https://onlinelibrary.wiley.com/terms-and-conditions) on Wiley Online Library for rules of use; OA articles are governed by the applicable Creative Commons License

gold(III) compounds $[PPh_4][(CF_3)_3AuI]$ and $[PPh_4][(CF_3)_3AuF]$,[19] as well as the linear gold(I) derivatives $[PPh_4][CF_3AuCl]$[42] and $[PPh_4][CF_3AuBr]$,[43] were prepared as described elsewhere. The salt $[Ph_3PCH_2Ph][(CF_3)_3AuCl]$ was prepared by addition of the equimolar amount of $[Ph_3PCH_2Ph]Cl$ to a solution of $(CF_3)_3Au{\cdot}OEt_2$[18] and was further transformed into $[Ph_3PCH_2Ph][(CF_3)_3AuF]$ as described for the $[PPh_4]^+$ salts.[19] All other reagents were purchased from standard commercial suppliers and used as received. Elemental analyses were carried out using a PerkinElmer 2400 CHNS/O Series II microanalyzer. IR spectra were recorded on neat solid samples using a PerkinElmer Spectrum FT-IR spectrometer (4000–450 cm^{-1}) equipped with an ATR device. ^{19}F NMR spectra were recorded at room temperature on a Bruker AV-400 spectrometer. Chemical shifts (δ_F in ppm) are given with respect to $CFCl_3$. Chemically inequivalent CF_3 groups are indicated as follows: CF_3-Au-CF_3 refers to the mutually *trans*-standing CF_3 groups (q = quartet), whereas CF_3-Au-X refers to the CF_3 group *trans* to the anionic X ligand (spt = septet). NMR parameters associated with the $[PPh_4]^+$ or $[Ph_3PCH_2Ph]^+$ cations are unexceptional and are therefore omitted. High-resolution mass spectra (HRMS) were registered using electrospray ionization (ESI) techniques on a MicroToF-Q (Bruker Daltonics) spectrometer, using sodium formate clusters as external reference. Thermogravimetric and differential thermal analyses (TGA/DTA) were performed using a SDT 2960 instrument at a heating rate of 10 °C min^{-1} under N_2 atmosphere.

Synthesis of $[PPh_4][(CF_3)_3Au(N_3)]$ (1). ***Method A***: NaN_3 (13 mg, 197 μmol) was added to a MeCN solution (5 mL) of $[PPh_4][(CF_3)_3AuF]$ (100 mg, 131 μmol) and the mixture was stirred at room temperature for 30 min. Removal of the solvent by vacuum evaporation afforded a white residue which was extracted with CH_2Cl_2 (10 mL). The extract was separated by filtration and the colorless filtrate was evaporated to dryness. Treatment of the resulting residue with Et_2O (3 mL) rendered a white solid, which was filtered, washed with more Et_2O (2×2 mL), vacuum dried and identified as compound **1** (75 mg, 95 μmol, 73% yield). ***Method B***: An equimolar amount of Me_3SiN_3 (18 μL, 131 μmol) was added to a CH_2Cl_2 solution (5 mL) of $[PPh_4][(CF_3)_3AuF]$ (100 mg, 131 μmol). After 30 min of stirring at room temperature, all volatiles were removed by evaporation under reduced pressure. Treatment of the resulting residue with Et_2O (3 mL) rendered a white solid, which was filtered, washed with additional Et_2O (2×2 mL), vacuum dried and identified as compound **1** (82 mg, 104 μmol, 80% yield). **IR** (ATR; Figure S1): $\tilde{\nu}/cm^{-1}$ = 3060 (w), 2061 (s, ν_a: NNN), 1826 (w), 1686 (w), 1585 (w), 1484 (m), 1437 (s), 1396 (w), 1340 (w), 1316 (w), 1287 (m), 1190 (w), 1157 (s), 1109 (s), 1069 (vs), 1047 (vs), 1026 (s), 996 (s), 931 (m), 849 (m), 754 (s), 721 (vs), 689 (vs), 615 (m), 586 (w), 524 (vs), 453 (m), 431 (w), 406 (m). **^{19}F NMR** (376.308 MHz, CD_2Cl_2, 298 K; Figure S3): δ_F/ppm = −29.87 (spt, 3F, $^4J(F,F)$ = 6.3 Hz; CF_3-Au-N_3), −38.07 ppm (q, 6F; CF_3-Au-CF_3). **HRMS** (ESI−): *m/z* calcd for $C_3AuF_9N_3$: 445.9620; found: 445.9602. **Elemental analysis** calcd (%) for $C_{27}H_{20}AuF_9N_3P$: C 41.29, H 2.57, N 5.35; found: C 41.27, H 2.59, N 5.44. **Single crystals** of $[Ph_3PCH_2Ph][(CF_3)_3Au(N_3)]$ (**1′**) suitable for X-ray diffraction were obtained by slow diffusion at 4 °C of a layer of *n*-hexane (2 mL) into a solution of compound **1′** in CH_2Cl_2 (1 mL), prepared starting from $[Ph_3PCH_2Ph][(CF_3)_3AuF]$ (15 mg, 19.3 μmol; see General Procedures) following method B.

Transformation of $[PPh_4][CF_3AuX]$ (X = Cl, Br) into $[PPh_4][CF_3Au(N_3)]$ (2). ***Method A***: An excess of NaN_3 (6 mg, 88 μmol) was added to a solution of $[PPh_4][CF_3AuBr]$ (30 mg, 44 μmol) in Me_2CO (3 mL) in the dark, and the mixture was stirred at room temperature for 3 h. Incomplete conversion was evidenced by ^{19}F NMR and MS (ESI−). ***Method B***: An excess of NaN_3 (92 mg, 1.40 mmol) was added to a solution of $[PPh_4][CF_3AuCl]$ (90 mg, 140 μmol) in Me_2CO (5 mL) in the dark and the mixture was stirred overnight at room temperature. Incomplete conversion was evidenced by ^{19}F NMR. Neither a greater excess of NaN_3 nor longer reaction times led to full conversion. The reaction mixture was eventually evaporated to dryness and the residue was extracted with CH_2Cl_2 (5 mL). The resulting suspension was filtered through high-quality diatomite. Solvent removal by vacuum evaporation afforded a white solid, which was suspended in Et_2O (3 mL), filtered, washed with additional Et_2O (2×2 mL) and vacuum dried. This solid consisted of a 3:1 mixture of the final compound **2** and the starting material,[42] respectively, as identified by ^{19}F NMR (Figure S4). **^{19}F NMR** of **2** (376.308 MHz, CD_2Cl_2, 298 K): δ_F/ppm = −21.91 (s, CF_3). **Single crystals** of **2** suitable for X-ray diffraction were obtained by slow diffusion at 4 °C of a layer of *n*-hexane (2 mL) into the obtained reaction mixture.

Synthesis of $[PPh_4][(CF_3)_3Au(ONO_2)]$ (3): An equimolar amount of $AgNO_3$ (20 mg, 115 μmol) was added to a solution of $[PPh_4][(CF_3)_3AuI]$ (100 mg, 115 μmol) in MeCN (5 mL) in the dark. After 30 min stirring, the reaction mixture was evaporated to dryness and the resulting residue was extracted with CH_2Cl_2 (10 mL). The suspension was filtered through high-quality diatomite to separate the AgI. Solvent removal in the extract by vacuum evaporation afforded a white solid, which was suspended in *n*-hexane (3 mL), filtered, washed with more *n*-hexane (2×2 mL), vacuum dried, and identified as compound **3** (73 mg, 91 μmol, 79% yield). **IR** (ATR; Figure S2): $\tilde{\nu}/cm^{-1}$ = 3065 (w), 1588 (w), 1510 (s, ν_a: NO_2), 1485 (m), 1443 (m), 1437 (m), 1341 (w), 1316 (w), 1289 (s, ν_s: NO_2), 1186 (w), 1169 (m, N–O), 1162 (m), 1109 (s), 1080 (vs), 1063 (vs), 1030 (s), 1028 (s), 996 (m), 984 (s), 929 (m), 847 (w), 796 (w), 761 (m), 754 (m), 746 (w), 722 (vs), 687 (vs), 616 (w), 524 (vs), 450 (m). **^{19}F NMR** (376.308 MHz, CD_2Cl_2, 298 K; Figure S5): δ_F/ppm = −27.53 (spt, 3F, $^4J(F,F)$ = 6.0 Hz; CF_3-Au-NO_3), −40.24 (q, 6F; CF_3-Au-CF_3). **HRMS** (ESI−): *m/z* calcd for $C_3AuF_9NO_3$: 465.9406; found: 465.9407. **Elemental analysis** calcd (%) for $C_{27}H_{20}AuF_9NO_3P$: C 40.27, H 2.50, N 1.74; found: C 40.32, H 2.38, N 1.60. **Single crystals** of the $[Ph_3PCH_2Ph][(CF_3)_3Au(NO_3)]$ salt (**3′**) suitable for X-ray diffraction were obtained by slow diffusion at 4 °C of a layer of *n*-hexane (2 mL) into a solution of compound **3′** in CH_2Cl_2 (1 mL), prepared by the same procedure starting from $[Ph_3PCH_2Ph][(CF_3)_3AuCl]$ (15 mg, 18.9 μmol; see General Procedures).

Multistage mass spectrometry (MS^n): ESI-ion trap mass spectra were recorded on a Bruker Esquire 3000+ spectrometer (Bruker Daltonics). Analyses were carried out in negative ion mode, with Smart Parameter Settings optimized for each *m/z* value. The nebulizer (N_2) gas pressure, drying gas (N_2) flow rate and drying gas temperature were kept at 0.7 bar, 4.0 dm^3 min^{-1} and 350 °C, respectively. Spectra were acquired in the *m/z* 50–1000 range, and the mass axis was externally calibrated with a tuning mix (from Agilent Technologies). 5 ppm solutions of the samples were transferred into the ESI source by means of a syringe pump at a flow rate of 4 mm^3 min^{-1}. ESI-CID-MS^n analyses were carried out using He as the collision gas and the amplitude voltage was optimized in each case to obtain the maximum fragment intensity. The obtained spectra are shown in Figures S6–S12. **Q-TOF MS^2 spectra**[23] were recorded on a Bruker MicroTOF-Q Spectrometer (Bruker Daltonics). The nebulizer (N_2) gas pressure, drying gas (N_2) flow rate and drying gas temperature were kept at 0.4 bar, 4.0 dm^3 min^{-1} and 180 °C, respectively. ESI-CID-MS^n analyses were carried out using N_2 as the collision gas, 15 eV collision energy, and an isolation width for the precursor ion of 5 *m/z* units. Whereas the N_3^- ion was absent in the spectra of compound **1**, the NO_3^- ion was actually observed in the spectra of compound **3**. This contrasting behaviour nicely correlates with the calculated energy required for each process (Schemes S1 and S2).

Crystal data and structure refinement: Crystal data and other details of the structure analysis are presented in Tables S1, S3 and S5. Single crystals suitable for X-ray diffraction studies were

© 2022 The Authors. Chemistry - A European Journal published by Wiley-VCH GmbH

15213765, 2023, 8, Downloaded from https://chemistry-europe.onlinelibrary.wiley.com/doi/10.1002/chem.202203181 by Universidad De Zaragoza, Wiley Online Library on [28/02/2023]. See the Terms and Conditions (https://onlinelibrary.wiley.com/terms-and-conditions) on Wiley Online Library for rules of use; OA articles are governed by the applicable Creative Commons License

obtained as indicated in the corresponding Experimental entry. Crystals were mounted at the end of quartz fibres. The radiation used in all cases was graphite-monochromated Mo–Kα ($\lambda =$ 71.073 pm). X-ray intensity data were collected on a Bruker Smart Apex (**1′** and **3′**) or a Bruker Apex Duo CCD (**2**) diffractometer. The diffraction frames were integrated and corrected from absorption by using the CrysAlis Pro program[44] (**1′** and **3′**) or by using the SAINT software[45] (**2**). Data collection was performed at 100 K in all cases. The structures were solved by Patterson and Fourier methods and refined by full-matrix least squares on F^2 with SHELXL.[46] All non-H atoms were assigned anisotropic displacement parameters and refined without positional constraints. The positions of the H atoms were constrained to idealised geometries and assigned isotropic displacement parameters equal to 1.2 times the U_{iso} values of their respective parent atoms. For **1′**, the F atoms of all three CF_3 ligands show rotational disorder over two positions, which were refined with the following partial occupancies: 0.52/0.48, 0.52/0.48 and 0.67/0.33. Restrains in the geometry and anisotropic thermal parameters were used for these F atoms. Full-matrix least-squares refinement of these models against F^2 converged to final residual indices given in Tables S1, S3 and S5.[20] Selected interatomic distances and angles are given in Tables S2, S4 and S6.

Computational details: Density Functional Theory (DFT) calculations were performed with the Gaussian09 package[47] at the M06 level of theory[48] with an ultrafine grid option. All atoms (C, N, O, F, and Au) have been described using Ahlrichs' def2-TZVPD, a Triple-Zeta-Valence basis set including Polarization and Diffuse basis functions[49] along with the corresponding quasi-relativistic pseudo-potential for Au atoms, as obtained from the Basis Set Exchange webpage.[50,51] The potential energy surfaces of the studied complexes and of the species involved in their fragmentation processes have been examined at this level of theory, and their geometries have been optimized in the gas phase with no symmetry restrictions. Frequency calculations have been performed in all the collected stationary points in order to check their nature of either minima or transition states. Atomic coordinates for all the optimized structures are included as a separate *.xyz* file in the Supporting Information.

Spin multiplicity analysis: As a first approach, the complexes of interest, $[(CF_3)_3AuN]^-$ (**AuN**) and $[(CF_3)_3AuO]^-$ (**AuO**), were analyzed at the referred DFT/M06/def2-TZVPD level of theory. Two possible spin states, triplet (^{3}**AuN**) and singlet (^{1}**AuN**), can be envisaged for the former, whereas a spin doublet is obtained for the latter: ^{2}**AuO**. The results obtained at this level for the **AuN** spinomers support the high-spin complex as the most energetically favored ($\Delta G^\circ = -33.9$ kcal mol^{-1}). Figure S15 shows the optimized structures for the ^{3}**AuN**, ^{1}**AuN**, and ^{2}**AuO** species together with the relative energies obtained for the **AuN** spinomers.

CASSCF calculations were additionally performed at the DFT ground state geometries of the open-shell **AuO** and **AuN** systems in the ORCA 4.2.1 software[52] to assess any possible multiconfigurational character. CASSCF wavefunctions were optimized using the ZORA approximation[53] along with the ZORA-def2-TZVP basis sets,[54] which include the segmented all-electron relativistically contracted SARC-ZORA-TZVP basis set for gold. General-purpose Coulomb fitting SARC/J auxiliary basis sets were also employed within the RI–J approximation. We chose an active space comprising 6 ligand-based orbitals for both **AuO** and **AuN** complexes, leading to CAS(9,6) and CAS(8,6) expansions, respectively. The active space was optimized averaging 7 doublets for **AuO** and 28 singlets and 21 triplets for **AuN**. The electronic ground state of **AuN** is practically monoconfigurational (Table S7) with the two unpaired electrons located in the b_2 and $2b_1$ MOs composed mainly of the $N(p_x)$ and $N(p_y)$ atomic orbitals, respectively (Figure S16). This is in good agreement with the DFT calculations discussed above, which predicted a triplet ground state being more stable by 33.9 kcal mol^{-1} than the corresponding singlet (Figure S15). On the other hand, for the **AuO** complex just two configurations account for 94% of the CAS wavefunction (Table S8), namely those placing the unpaired electron in the MOs $1b_1$ and $2b_1$, respectively (Figure S17). These MOs have the same symmetry (B_1, C_{2v} point group) and are $O\cdots C_{cis}$ bonding and antibonding combinations of the $O(p_x)$ AO with the out-of-phase combination of the lone pairs of the two *cis* ligands. In those two MOs, the $O(p_x)$ AO mixes with the σ* orbitals of the CF_3 groups *cis* to O leading to the two $O–C_{cis}$ bonding and antibonding combinations. The CAS procedure, when mixing the two configurations, uncouples the C-based orbitals, leaving the unpaired electron largely at the O(p) AO. It is worth noting that this is in line with the spin-density distribution calculated at the DFT level (Figure 1b). Accordingly, if we come back to our single-determinant DFT calculations, it can be seen that the spin density in the C atoms *cis* to O is located on α orbitals while in the remaining C atom (*trans* to O) it is located in β orbitals, which confirms the spin delocalization[55] onto the C atoms of the two equivalent CF_3 ligands *cis* to O and some degree of spin polarization towards the C atom of the CF_3 ligand *trans* to O.

Acknowledgements

This work was supported by the Spanish MICIU/FEDER (Projects PID2021-122869NB-I00 and PGC2018-093863-B–C21), the Gobierno de Aragón (Grupo E17_20R) and the Structures of Excellence María de Maeztu program (MDM-2017-0767). BIFI (Instituto de Biocomputación y Física de Sistemas Complejos) and CESGA (Centro de Supercomputación de Galicia) are acknowledged for allocation of computational resources. J.E. is grateful to the Spanish MICCIN for a Ramón y Cajal research contract (RYC-2017-22853) and A.P.-B. thanks the Spanish MECD for a grant (FPU15/03940).

Conflict of Interest

The authors declare no conflict of interest.

Data Availability Statement

The data that support the findings of this study are available in the supplementary material of this article.

Keywords: inverted ligand field · nitrene · organogold · oxyl · radicals

[1] Y. Gong, M. Zhou, L. Andrews, *Chem. Rev.* **2009**, *109*, 6765.
[2] D. Schröder, H. Schwarz, S. Shaik, *Struct. Bonding (Berlin)* **2000**, *97*, 91.
[3] a) H. B. Gray, J. R. Winkler, *Acc. Chem. Res.* **2018**, *51*, 1850; b) J. R. Winkler, H. B. Gray, *Struct. Bonding (Berlin)* **2012**, *142*, 17; c) J. M. Mayer, *Comments Inorg. Chem.* **1988**, *8*, 125.
[4] J. D. Rolfes, M. van Gastel, F. Neese, *Inorg. Chem.* **2020**, *59*, 1556.
[5] R. S. Hay-Motherwell, G. Wilkinson, B. Hussain-Bates, M. B. Hursthouse, *Polyhedron* **1993**, *12*, 2009.
[6] PNP = N(CHCHP*t*Bu$_2$)$_2$: D. Delony, M. Kinauer, M. Diefenbach, S. Demeshko, C. Würtele, M. C. Holthausen, S. Schneider, *Angew. Chem. Int. Ed.* **2019**, *58*, 10971; *Angew. Chem.* **2019**, *131*, 11087.

© 2022 The Authors. Chemistry - A European Journal published by Wiley-VCH GmbH

15213765, 2023, 8, Downloaded from https://chemistry-europe.onlinelibrary.wiley.com/doi/10.1002/chem.202203181 by Universidad De Zaragoza, Wiley Online Library on [28/02/2023]. See the Terms and Conditions (https://onlinelibrary.wiley.com/terms-and-conditions) on Wiley Online Library for rules of use; OA articles are governed by the applicable Creative Commons License

[7] a) I. Efremenko, E. Poverenov, J. M. L. Martin, D. Milstein, *J. Am. Chem. Soc.* **2010**, *132*, 14886; b) E. Poverenov, I. Efremenko, A. I. Frenkel, Y. ben David, L. J. W. Shimon, G. Leitus, L. Konstantinovski, J. M. L. Martin, D. Milstein, *Nature* **2008**, *455*, 1093.
[8] a) C. Limberg, *Angew. Chem. Int. Ed.* **2009**, *48*, 2270; *Angew. Chem.* **2009**, *121*, 2305; b) C. L. Hill, *Nature* **2008**, *455*, 1045.
[9] G. Wang, M. Zhou, J. T. Goettel, G. J. Schrobilgen, J. Su, J. Li, T. Schlöder, S. Riedel, *Nature* **2014**, *514*, 475.
[10] a) L. Wolański, M. A. Domański, W. Grochala, P. Szarek, *Chem. Commun.* **2020**, *56*, 13137; b) S.-X. Hu, W.-L. Li, J.-B. Lu, J. L. Bao, H. S. Yu, D. G. Truhlar, J. K. Gibson, J. Marçalo, M. Zhou, S. Riedel, W. H. E. Schwarz, J. Li, *Angew. Chem. Int. Ed.* **2018**, *57*, 3242; *Angew. Chem.* **2018**, *130*, 3297.
[11] K. P. Kepp, *Inorg. Chem.* **2016**, *55*, 9461.
[12] A short excursion into molecular gold compounds containing terminal AuO units was unsuccessful: K. P. O'Halloran, C. Zhao, N. S. Ando, A. J. Schultz, T. F. Koetzle, P. M. B. Piccoli, B. Hedman, K. O. Hodgson, E. Bobyr, M. L. Kirk, S. Knottenbelt, E. C. Depperman, B. Stein, T. M. Anderson, R. Cao, Y. V. Geletii, K. I. Hardcastle, D. G. Musaev, W. A. Neiwert, X. Fang, K. Morokuma, S. Wu, P. Kögerler, C. L. Hill, *Inorg. Chem.* **2012**, *51*, 7025.
[13] H.-J. Zhai, C. Bürgel, V. Bonačić-Koutecký, L.-S. Wang, *J. Am. Chem. Soc.* **2008**, *130*, 9156.
[14] a) L. Li, H. Beckers, T. Stüker, T. Lindič, T. Schlöder, D. Andrae, S. Riedel, *Inorg. Chem. Front.* **2021**, *8*, 1215; b) L. Li, T. Stüker, S. Kieninger, D. Andrae, T. Schlöder, Y. Gong, L. Andrews, H. Beckers, S. Riedel, *Nat. Commun.* **2018**, *9*, 1267.
[15] M. Willis, M. Götz, A. K. Kandalam, G. F. Ganteför, P. Jena, *Angew. Chem. Int. Ed.* **2010**, *49*, 8966; *Angew. Chem.* **2010**, *122*, 9150.
[16] G. K. Koyanagi, D. Caraiman, V. Blagojevic, D. K. Bohme, *J. Phys. Chem. A* **2002**, *106*, 4581.
[17] PNP=N(CHCHP*t*Bu$_2$)$_2$: J. Sun, J. Abbenseth, H. Verplancke, M. Diefenbach, B. de Bruin, D. Hunger, C. Würtele, J. van Slageren, M. C. Holthausen, S. Schneider, *Nat. Chem.* **2020**, *12*, 1054.
[18] A. Pérez-Bitrián, M. Baya, J. M. Casas, L. R. Falvello, A. Martín, B. Menjón, *Chem. Eur. J.* **2017**, *23*, 14918.
[19] A. Pérez-Bitrián, S. Martínez-Salvador, M. Baya, J. M. Casas, A. Martín, B. Menjón, J. Orduna, *Chem. Eur. J.* **2017**, *23*, 6919.
[20] Deposition Numbers 2180331 (for **1'**), 2180332 (for **2**) and 2180333 (for **3'**) contain the supplementary crystallographic data for this paper. These data are provided free of charge by the joint Cambridge Crystallographic Data Centre and Fachinformationszentrum Karlsruhe Access Structures service.
[21] D. Joven-Sancho, M. Baya, L. R. Falvello, A. Martín, J. Orduna, B. Menjón, *Chem. Eur. J.* **2021**, *27*, 12796
[22] R. Haiges, M. Rahm, D. A. Dixon, E. B. Garner, III, K. O. Christe, *Inorg. Chem.* **2012**, *51*, 1127.
[23] Given that the MS^2 low-mass cut-off of ion-trap analyzers prevents the detection of light anions (see Ref. [24]), the MS^2 experiments were also performed using a Q-TOF instrument (see Experimental) in order to detect the presence of N_3^- or NO_3^- formed by ionic dissociation.
[24] R. E. March, J. F. J. Tod: *Quadrupole Ion Trap Mass Spectrometry*, 2nd ed., Wiley, Hoboken NJ, **2005**.
[25] C&N = 2-(2'-pyridyl)phenyl: D. Fan, E. Meléndez, J. D. Ranford, P. F. Lee, J. J. Vittal, *J. Organomet. Chem.* **2004**, *689*, 2969.
[26] a) A. G. Algarra, V. V. Grushin, S. A. Macgregor, *Organometallics* **2012**, *31*, 1467; b) P. Sgarbossa, A. Scarso, G. Strukul, R. A. Michelin, *Organometallics* **2012**, *31*, 1257; c) T. G. Appleton, H. C. Clark, L. E. Manzer, *Coord. Chem. Rev.* **1973**, *10*, 335.
[27] M. S. Wickleder, F. Gerlach, S. Gagelmann, J. Bruns, M. Fenske, K. Al-Shamery, *Angew. Chem. Int. Ed.* **2012**, *51*, 2199; *Angew. Chem.* **2012**, *124*, 2242.
[28] M. S. Wickleder, O. Büchner, F. Gerlach, M. Necke, K. Al-Shamery, T. Wich, T. Luttermann, *Chem. Mater.* **2008**, *20*, 5181.
[29] C. D. Garner, S. C. Wallwork, *J. Chem. Soc. A* **1970**, 3092.
[30] K. B. Borisenko, M. Kolonits, B. Rozsondai, I. Hargittai, *J. Mol. Struct.* **1997**, *413–414*, 121.
[31] J. D. Atwood, *Inorganic and Organometallic Reaction Mechanisms*, 2nd ed., VCH, New York, **1997**, Sect. 3.3, 80–82.
[32] B. P. Dailey, J. N. Shoolery, *J. Am. Chem. Soc.* **1955**, *77*, 3977.
[33] H. Oberhammer, *J. Mol. Struct.* **2002**, *605*, 177.
[34] A. Hammerl, T. M. Klapötke, in *Encyclopedia of Inorganic Chemistry* (Ed.: R. B. King), Wiley, Chichester (UK), **2005**, 3531–3600.
[35] Even the highly unstable $IONO_2$ has been considered as a potential reservoir for atmospheric iodine with a predicted lifetime of the order of 6 h: P. Marshall, *Adv. Quantum Chem.* **2008**, *55*, 159.
[36] a) P. Schwerdtfeger, O. R. Smits, P. Pyykkö, *Nat. Chem. Rev.* **2020**, *4*, 359; b) P. Schwerdtfeger, M. Lein, in *Gold Chemistry: Applications and Future Directions in the Life Sciences* (Ed.: F. Mohr), Wiley-VCH, Weinheim, **2009**, Ch. 4, 183–247.
[37] a) P. Karen, P. McArdle, J. Takats, *Pure Appl. Chem.* **2016**, *88*, 831; b) P. Karen, *Angew. Chem. Int. Ed.* **2015**, *54*, 4716; *Angew. Chem.* **2015**, *127*, 4798.
[38] Metal-oxyl derivatives are key species in hydrogen-atom transfer (HAT) processes, including C–H bond activation: a) H. Schwarz, S. Shaik, J. Li, *J. Am. Chem. Soc.* **2017**, *139*, 17201; b) B. Mondal, L. Roy, F. Neese, S. Ye, *Isr. J. Chem.* **2016**, *56*, 763; c) N. Dietl, M. Schlangen, H. Schwarz, *Angew. Chem. Int. Ed.* **2012**, *51*, 5544; *Angew. Chem.* **2012**, *124*, 5638.
[39] The strongly oxidizing Ag(II) center is known to induce a similar hole shift to oxides: W. Grochala, *J. Fluorine Chem.* **2008**, *129*, 82.
[40] R. Hoffmann, S. Alvarez, C. Mealli, A. Falceto, T. J. Cahill, III, T. Zeng, G. Manca, *Chem. Rev.* **2016**, *116*, 8173.
[41] a) A. Pérez-Bitrián, M. Baya, J. M. Casas, A. Martín, B. Menjón, *Dalton Trans.* **2021**, *50*, 5465; b) M. Baya, D. Joven-Sancho, P. J. Alonso, J. Orduna, B. Menjón, *Angew. Chem. Int. Ed.* **2019**, *58*, 9954; *Angew. Chem.* **2019**, *131*, 10059; c) I. M. DiMucci, J. T. Lukens, S. Chatterjee, K. M. Carsch, C. J. Titus, S. J. Lee, D. Nordlund, T. A. Betley, S. N. MacMillan, K. M. Lancaster, *J. Am. Chem. Soc.* **2019**, *141*, 18508.
[42] M. Baya, A. Pérez-Bitrián, S. Martínez-Salvador, J. M. Casas, B. Menjón, J. Orduna, *Chem. Eur. J.* **2017**, *23*, 1512.
[43] S. Martínez-Salvador, L. R. Falvello, A. Martín, B. Menjón, *Chem. Sci.* **2015**, *6*, 5506.
[44] *CrysAlis Pro* 1.171.39.44a, Rigaku Oxford Diffraction **2018**.
[45] SAINT+ v. 6.02, Bruker Analytical X-ray Systems, Madison, WI, **1999**.
[46] SHELXL Version 2014/8: G. M. Sheldrick, *Acta Crystallogr. Sect. C* **2015**, *71*, 3.
[47] M. J. Frisch, G. W. Trucks, H. B. Schlegel, G. E. Scuseria, M. A. Robb, J. R. Cheeseman, G. Scalmani, V. Barone, B. Mennucci, G. A. Petersson, H. Nakatsuji, M. Caricato, X. Li, H. P. Hratchian, A. F. Izmaylov, J. Bloino, G. Zheng, J. L. Sonnenberg, M. Hada, M. Ehara, K. Toyota, R. Fukuda, J. Hasegawa, M. Ishida, T. Nakajima, Y. Honda, O. Kitao, H. Nakai, T. Vreven, J. A. Montgomery, Jr., J. E. Peralta, F. Ogliaro, M. Bearpark, J. J. Heyd, E. Brothers, K. N. Kudin, V. N. Staroverov, T. Keith, R. Kobayashi, J. Normand, K. Raghavachari, A. Rendell, J. C. Burant, S. S. Iyengar, J. Tomasi, M. Cossi, N. Rega, J. M. Millam, M. Klene, J. E. Knox, J. B. Cross, V. Bakken, C. Adamo, J. Jaramillo, R. Gomperts, R. E. Stratmann, O. Yazyev, A. J. Austin, R. Cammi, C. Pomelli, J. W. Ochterski, R. L. Martin, K. Morokuma, V. G. Zakrzewski, G. A. Voth, P. Salvador, J. J. Dannenberg, S. Dapprich, A. D. Daniels, O. Farkas, J. B. Foresman, J. V. Ortiz, J. Cioslowski, D. J. Fox; *Gaussian 09, Revision D.01* Gaussian, Inc., Wallingford CT, **2013**.
[48] Y. Zhao, D. G. Truhlar, *Theor. Chem. Acc.* **2008**, *120*, 215.
[49] a) D. Rappoport, F. Furche, *J. Chem. Phys.* **2010**, *133*, 134105; b) F. Weigend, R. Ahlrichs, *Phys. Chem. Chem. Phys.* **2005**, *7*, 3297; c) K. A. Peterson, D. Figgen, E. Goll, H. Stoll, M. Dolg, *J. Chem. Phys.* **2003**, *119*, 11113; d) D. Andrae, U. Häußermann, M. Dolg, H. Stoll, H. Preuß, *Theor. Chim. Acta* **1990**, *77*, 123.
[50] Basis Set Library obtained from: https://www.basissetexchange.org.
[51] a) B. P. Pritchard, D. Altarawy, B. Didier, T. D. Gibson, T. L. Windus, *J. Chem. Inf. Model.* **2019**, *59*, 4814; b) D. Feller, *J. Comput. Chem.* **1996**, *17*, 1571; c) K. L. Schuchardt, B. T. Didier, T. Elsethagen, L. Sun, V. Gurumoorthi, J. Chase, J. Li, T. L. Windus, *J. Chem. Inf. Model.* **2007**, *47*, 1045.
[52] F. Neese, *WIREs Comput. Mol. Sci.* **2018**, *8*, e1327.
[53] C. van Wüllen, *J. Chem. Phys.* **1998**, *109*, 392.
[54] D. A. Pantazis, X.-Y. Chen, C. R. Landis, F. Neese, *J. Chem. Theory Comput.* **2008**, *4*, 908.
[55] a) E. Ruiz, J. Cirera, S. Alvarez, *Coord. Chem. Rev.* **2005**, *249*, 2649; b) J. Cano, E. Ruiz, S. Alvarez, M. Verdaguer, *Comments Inorg. Chem.* **1998**, *20*, 27.

Manuscript received: October 12, 2022
Accepted manuscript online: October 20, 2022
Version of record online: December 16, 2022

© 2022 The Authors. Chemistry - A European Journal published by Wiley-VCH GmbH

15213765, 2023, 8, Downloaded from https://chemistry-europe.onlinelibrary.wiley.com/doi/10.1002/chem.202203181 by Universidad De Zaragoza, Wiley Online Library on [28/02/2023]. See the Terms and Conditions (https://onlinelibrary.wiley.com/terms-and-conditions) on Wiley Online Library for rules of use; OA articles are governed by the applicable Creative Commons License